^{1}H HYPERFINE INTERACTIONS IN THE Mn-CLUSTER OF PHOTOSYSTEM II IN THE S_2 STATE DETECTED BY HYPERFINE SUBLEVEL CORRELATION SPECTROSCOPY

Jesús I. Martínez[1,], Inmaculada Yruela[2], Rafael Picorel[2] and Pablo J. Alonso[1],*

[1]Instituto de Ciencia de Materiales de Aragón (ICMA), Consejo Superior de Investigaciones Científicas-Universidad de Zaragoza. C/ Pedro Cerbuna 12, E-50009 Zaragoza, Spain.

[2]Estación Experimental de Aula Dei, Consejo Superior de Investigaciones Científicas. Avda. Montañana, 1005, E-50059 Zaragoza, Spain.

* Corresponding author

Telephone number: +34 976762460

FAX number: +34 976761229

e-mail address: jimartin@unizar.es

TITLE RUNNING HEAD: ^{1}H hyperfine interactions in the Mn-cluster

ABSTRACT

A study of the hydrogen hyperfine couplings of the Mn-cluster of the oxygen-evolving complex of Photosystem II in the S_2 state of the Kok cycle by means of Hyperfine Sublevel Correlation Spectroscopy was achieved. Features corresponding to hyperfine interaction of at least two hydrogen nuclei were detected. Combining our results with previous ENDOR data, hyperfine constants were determined, and using a model for the structure and electronic spin state of the Mn-cluster relevant structural information of the S_2 state was obtained. This new information can be used for improving our knowledge about the structure and function of the Mn-cluster during light-driven water oxidation reaction in oxygenic photosynthetic organisms.

KEYWORDS: EPR, ESEEM, HYSCORE, Photosynthesis

INTRODUCTION

Oxygen-evolving complex (OEC) is the part of the Photosystem II (PS II) where the light-driven water oxidation takes place in cyanobacteria, green algae and higher plants. The water oxidation proceeds through a cycle of (at least) five steps known as *Kok cycle*. Each step is identified as a S_i (i = 0 to 4) state and is characterized, among other structural and electronic changes, by a specific oxidation state of a cluster of four Mn atoms (Mn-cluster). This cluster is believed to catalyse the water-oxidation process within the OEC. The atomic and electronic structure of the Mn-cluster in each S_i state has been extensively studied, as they are considered key features for understanding its function. However, many questions still remain unresolved. In the last years, different structural data from X-ray diffraction, EXAFS, and theoretical chemistry have been used to obtain a structural model, but the evidence seems to be difficult to reconcile[1-3]. Similarly, several models have been proposed for the electronic structure of the Mn-cluster with different number of Mn atoms, oxidation numbers, spin states or exchange coupling schemes[4-7]. Additionally, the role of a Ca^{2+} and a Cl^- ions in the Mn-cluster structure and function is under discussion. Other interesting questions are when and how the catalytic water molecules enter the Mn-cluster environment[5,6,8].

Electron Paramagnetic Resonance (EPR) techniques have given useful information on the structure and spin state of the Mn-cluster. Continuous wave (CW) EPR spectra of S_o, S_1, S_2 and S_3 states of the cluster have been reported[9,10]. For S_o and S_2, the hyperfine splitting of the CW-EPR signals has been interpreted as due to interaction of the total electronic spin with the ^{55}Mn nuclei. A model that related the exchange coupling scheme with the measured hyperfine splitting was developed[4,11,12], and the estimation of the hyperfine coupling of the four ^{55}Mn nuclei from CW-EPR and Electron Nuclear Double Resonance (ENDOR) measurements allowed determination of a quite detailed picture of the electronic structure of the Mn-cluster in S_o and S_2 states[7,13]. For the S_2 state, the total spin is S_T = ½, and it comes from a strongly exchange coupled system formed by three Mn(IV) centers and one Mn(III). Several coupling schemes have been considered compatible with the experimental evidence. Among them, the "trimer-monomer" scheme (also known as "Dangler model") has received much attention in

the last years, as it seems to be supported from other structural data[3,4,14]. Nevertheless, some details of the model, as the precise values of the exchange coupling constants and the actual position of the Mn(III) center within the cluster, remain unresolved.

EPR techniques are also suitable for detecting (weak) hyperfine couplings between the electronic spin and hydrogen nuclei from water, thus giving details on the OEC water oxidation process. Accordingly, several ^{1}H-ENDOR and Electron Spin Echo Envelope Modulation (ESEEM) measurements of the Mn-cluster in the S_2 state have been reported[15-19]. Spectral features associated with ^{1}H hyperfine coupling were indeed detected. Unfortunately, there are several signals in the spectra that are not clearly resolved, and some others are very weak. Consequently, the number of ^{1}H nuclei and hyperfine constants used by different groups for interpreting the results are not the same. The problem of assigning ENDOR and one-dimensional (1D) ESEEM signals in orientationally disordered samples with many anisotropic hyperfine couplings is common in biological paramagnetic systems. Two-dimensional (2D) ESEEM techniques can resolve it as the superimposed 1D signals become well separated in a 2D spectrum. In particular, Hyperfine Sublevel Correlation Spectroscopy (HYSCORE), which is a 2D ESEEM technique based on a four pulse sequence, has demonstrated to be useful to characterize hyperfine coupling in orientationally disordered samples of biological systems[20-22].

Having these ideas in mind, in this paper we present a study of the ^{1}H hyperfine interactions with the Mn-cluster of PSII in the S_2 state by means of HYSCORE experiments. From the combined analysis of our results and previously reported ENDOR measurements, hyperfine constants for at least two ^{1}H nuclei were obtained. These constants could offer valuable insights about the presence of water molecules in the structure of the Mn-cluster in the S_2 state of the Kok cycle. The information obtained from our measurements should be taken into account, in combination with other evidences from X-ray diffraction, EXAFS, CW-EPR, ^{55}Mn ENDOR, mass spectrometry and others, for establishing a suitable model for the Mn-cluster structure and function.

EXPERIMENTAL METHODS

Preparation of PSII samples in S_1 and S_2 states

Highly-enriched oxygen-evolving PSII membranes were isolated from market spinach according to [22,23]. Samples were suspended in 0.4 M sucrose, 15 mM NaCl, 5 mM $MgCl_2$ and 50 mM 2-(N-morpholino)ethanesulfonic acid (Mes)-NaOH, pH 6.0. PSII membranes exhibited oxygen evolution rates of 480 ± 30 (μmol O_2) (mg Chl)$^{-1}$ h^{-1} using 2,6-dichloro-benzoquinone (DCBQ) as artificial electron acceptor. PSII membranes samples at ~10 mg Chl/mL were frozen in liquid nitrogen and stored at -80ºC until use.

The S_1 state was generated in PSII samples inside quartz tubes (707-SQ from Wilmad Labglass) by annealing in the dark at room temperature for several minutes. S_2 state was generated by illumination at low temperature (200 K). A 24V-250W tungsten halogen lamp was used as the white light excitation source. The light beam was focalised on the sample for about 90 s. S_2 state was reached as the CW-EPR spectra of illuminated samples showed the typical multiline (MLS) feature[24]. Subsequently, samples were kept at liquid nitrogen temperature and transferred into the resonant cavity without significant warm up.

HYSCORE measurements

The measurements were performed in a Bruker ESP380E spectrometer working at X-band. The HYSCORE measurements were typically performed at 5 K. A liquid helium refrigerated Oxford CF935 continuous-flow cryostat was used. The four-pulse sequence ($\pi/2$ -τ - $\pi/2$ – t_1 - π - t_2 - $\pi/2$ - τ), with t_1 and t_2 varying independently, was used for HYSCORE experiments. Sampling time, Δt, was typically 16 ns (Nyquist frequency 31.25 MHz). Spectra consisting of an array of 120×120 points were performed for different τ values using an appropriated 8-step phase cycling in order to minimize unwanted echoes. Finally, a value of τ = 200 ns was chosen since it enhances the proton signal intensity. The raw 2D time domain spectra were processed using the WINEPR software from Bruker. A two-dimensional Fourier transform was performed after subtracting the background decay modelled by a polynomial function of

third degree followed by a zero-filling to 256 points in each dimension and tapering with a Hamming window. The spectra shown correspond to the magnitude of the frequency-domain signals.

HYSCORE simulations

For spectra simulation we used a computer program developed in our laboratory. An isotropic electronic *g*-factor was assumed[25] and the effective spin formalism[26] was used. As we are interested in ^{1}H transitions, the nuclear spin Hamiltonian for each electronic spin manifold ($< S_z > = \pm ½$) contains the nuclear Zeeman and the hyperfine contributions. The input parameters for the computer simulation program were: the applied magnetic field strength, τ value, the Nyquist frequency, and the hyperfine coupling constants. Uniformly distributed values for the molecular orientation, typically more than 10^6, covering the whole sphere were taken. The nuclear frequencies and nuclear wave functions in each electronic spin manifold were calculated for different orientations of the magnetic fields by diagonalizing the nuclear Hamiltonian. The HYSCORE signal was calculated using the general expression given by Schweiger and Jeschke[21]. The obtained HYSCORE spectra consisted of an array of 513×257 equally spaced points in the (ω_1, ω_2) plane.

Model for the ^{1}H hyperfine interaction

The model for understanding the experimental hyperfine constant as a function of the spatial distribution of the Mn atoms and the ^{1}H nuclei is based on previous descriptions[7,13,16]. A hyperfine contribution to the Spin Hamiltonian like the following gives account of the experimental results:

$$^{hf}H(^1H) = \boldsymbol{S_T}\,\boldsymbol{\Sigma_i}\,(^{\boldsymbol{H}}\boldsymbol{A})_i\,(^{\boldsymbol{H}}\boldsymbol{I})_i \qquad (1)$$

where $\boldsymbol{S_T}$ is the total effective electronic spin $\boldsymbol{S_T}$ =1/2, $(^{\boldsymbol{H}}\boldsymbol{I})_i$ are the nuclear spin of each ^{1}H nucleus ($^{\boldsymbol{H}}\boldsymbol{I}$ =1/2), and $(^{\boldsymbol{H}}\boldsymbol{A})_i$ are the total hyperfine tensors for each ^{1}H nucleus. These hyperfine tensors can be calculated as:

$$(^{\boldsymbol{H}}\boldsymbol{A})_i = \boldsymbol{\Sigma_j}\,\rho_j\,(^{\boldsymbol{H}}\boldsymbol{a})_{ji} \qquad \text{(j from 1 to 4)} \qquad (2)$$

where $(^{H}\boldsymbol{a})_{ji}$ are the hyperfine tensors of the i-th ^{1}H nuclear spin with the j-th individual Mn electronic spin, and ρ_j is the "projection constant" of the total electronic spin on the j-th Mn atom[7,13]. When the nucleus and the atom are about 2.4 Å away or farther, the $(^{H}\boldsymbol{a})_{ji}$ tensors can be easily calculated in the "point dipole approximation"[21]. In such a case, $(^{H}\boldsymbol{a})_{ji}$ tensors are axial, with the principal direction z corresponding to the segment joining the Mn atom and the ^{1}H nucleus positions, with principal value

$$(^{H}a)_{ji}^{\,z} = 2\,(g_e\mu_e g_N\mu_N / r_{ji}^{\,3}) \qquad (3)$$

where r_{ji} is the distance between the j-th Mn atom and the i-th ^{1}H nucleus, and

$$g_e\mu_e g_N\mu_N = 79\ MHz\ \text{Å}^3 \qquad (4)$$

for a ^{1}H nucleus. The two other principal directions x and y lie on the normal plane to Mn-^{1}H segment, and their principal values are both

$$(^{H}a)_{ji}^{\,x,\,y} = -\,(c/r_{ji}^{\,3}) \qquad (5)$$

Note that, although in this approximation all the $(^{H}\boldsymbol{a})_{ji}$ tensors are axial, it does not necessarily have to be so for each $(^{H}\boldsymbol{A})_{i}$, as the principal directions of the four $(^{H}\boldsymbol{a})_{ji}$ tensors contributing to it (see eq. 2) are in principle different.

Calculation of hyperfine constants for ^{1}H nuclei

A FORTRAN computer program was developed in our laboratory for calculating hyperfine constants of ^{1}H nuclei as a function of their position with respect to the Mn-cluster model. This program makes use of the "point dipole approximation". The hyperfine interaction tensor is calculated by adding the contribution of the spin populations at each Mn-atom. The obtained (3 x 3) matrix is then diagonalized

to obtain the hyperfine constants. The program can be used to detect the positions of ^{1}H nuclei compatible with some given hyperfine constants, or to obtain the hyperfine constants for a given position. The input parameters for the computer simulation program are the number (2 or 4), positions and assigned projection constants of the Mn atoms.

RESULTS

HYSCORE experiments

The conventional illumination at 200 K from the dark stable S_1 state was used for obtaining the S_2 state of the PSII samples. Advancement to the S_2 state could easily be monitored by CW-EPR as the MLS in the $g \approx 2.00$ region was detected. The stable Y_D radical signal was also detected in CW-EPR spectra of both S_1 and S_2 states. For HYSCORE measurements, several magnetic field positions within the MLS region, but far enough from the Y_D signal, were selected (see Supporting Information, figure S1). HYSCORE spectra showed no trace of Y_D features[27], but several ones corresponding to the cytochrome (Cyt*) b_{559}* center appeared[22]. The HYSCORE features associated to the Mn-cluster S_2 state were those that have not been previously reported for Cyt b_{559} and Y_D[22,27], and that appeared only in the S_2 state spectra (see Supporting Information for spectral comparison). Such HYSCORE features were in the ^{1}H interaction region. As the contribution of the HYSCORE spectra for the S_1 state in this region was negligible, no subtraction of these spectra from the S_2 ones was necessary. These features are shown (Figures 1A and 1B) for two magnetic field values (338 mT and 370 mT). They consist in weak correlation signals close to the diagonal of the spectrum at the ^{1}H Larmor frequency of the positive quadrant. All these signals were just detected for a narrow range of τ values around 200 ns. They can be described as two correlation signals (numbered **1** and **2** in Figure 1A and 1B) symmetric with respect to the quadrant diagonal. They are better resolved in spectrum at 338 mT (Figure 1A), where signal **1** displays the shape of a quite narrow ridge, nearly perpendicular to the diagonal, spanning from (12.4 MHz, 16.6 MHz) to (13.8 MHz, 15.2 MHz). Signal **2** shows a quite different shape. Their correlations ridges are broader and are not perpendicular to the diagonal. Two blue lines are drawn in Figure 1A to show the approximated limits of the ridge widths. Although signals **1** and **2** are partially superimposed,

their different directions and widths allow them to be distinguished. Signals **1** and **2** could also be identified in HYSCORE spectra at other field positions, although they displayed even weaker features. In the spectrum at 370 mT (Figure 1B) signals **1** and **2** are not displayed as ridges, but just as peaks above the noise level in the highest intensity positions. Very weak evidences of signals 1 and 2 were also detected at other positions between 310 mT and 390 mT (data not shown). Additionally, the diagonal feature around the ^{1}H Larmor frequency is quite more intense in S_2 than in S_1 HYSCORE spectra (see Figures S2 to S5 in Supporting Information). Although a part of these features are due to unwanted 3-pulse echoes, the diagonal feature is an indication of "remote" ^{1}H nuclei (i. e., ^{1}H nuclei showing very weak hyperfine coupling).

For the analysis of signals **1** and **2** we made use of comparisons with previous ^{1}H ENDOR results. It was thus convenient to obtain the profiles of the HYSCORE features on each frequency axis (usually known as *skyline projections*). We eliminated all the correlations and diagonal features of the 2D HYSCORE spectrum, except signal **1** or signal **2**, and then we obtained the *skyline projections* in ω_1 and ω_2 axes (Figure 2). They were compared with previously reported ENDOR spectra[15-17,19], taking into account the different intensities of the signals obtained from the two techniques (see below).

Analysis of the spectral features

First estimation of hyperfine parameters from correlation ridges

Signals **1** and **2** were both assigned to hyperfine interactions of the Mn-cluster electronic spin with ^{1}H nuclei. In HYSCORE experiments of orientationally disordered samples, correlations corresponding to a ^{1}H axial hyperfine interaction display rather narrow ridges, which follow straight segments when the 2D frequency spectrum is represented in a (ω_1^2, ω_2^2) plot. When the ^{1}H hyperfine interaction is rhombic, correlations show triangle shape in the (ω_1^2, ω_2^2) plot. The triangle sides or the segment orientations are related with the hyperfine constants, and allow estimating them in each case[20,28]. Parts of the correlations (triangle or segment shaped) are usually lost because of small or no intensity of the HYSCORE signal for some orientations of the paramagnetic center, especially when the signal is weak. This causes inaccuracy in the estimation of the hyperfine constants or even prevents any significant

estimation, when the segment or triangle shapes cannot properly be identified. Nevertheless, a rhombic interaction may be inferred when the detected ridges are broad.

In our case, ridges of signal **1** were short but enough for a first estimation of the hyperfine parameters. They correspond to an axial hyperfine interaction, characterized by the isotropic, a, and the anisotropic, T, contributions[20,28], with a ^{1}H nucleus, hereafter called $^1H_1$, with two compatible sets of parameters:

$$\text{i) } T_1 = +2.9 \pm 0.5 \text{ MHz} \quad a_1 = -4.2 \pm 1.5 \text{ MHz} \qquad \textit{or} \qquad \text{ii) } T_1 = +2.9 \pm 0.5 \text{ MHz} \quad a_1 = +1,3 \pm 2.5 \text{ MHz} \tag{6}$$

where the two different principal values of the hyperfine tensor are $(A_{||})_1 = a_1 + 2\ T_1$, $(A_\perp)_1 = a_1 - T_1$. The ridge orientation allowed determination of the extremal values of the hyperfine interaction, but the uncertainty of assigning those values to $A_{||}$ or $A_\perp$ made these two sets compatible[20]. Even two additional sets would be compatible, corresponding to a simultaneous change of the signs of a and T, although in the following we only show the results with $T > 0$.

The error values were estimated form the HYSCORE signal width, that causes the inaccuracy of the parameters determining the straight segment in the (ω_1^2, ω_2^2) plot. It is seen that the anisotropic constant T_1 is obtained with a fair accuracy, whereas a_1 estimation is quite inaccurate.

As signal **2** displayed a feature broader than a single ridge, we assigned it to a rhombic hyperfine interaction with another ^{1}H nucleus, called $^1H_2$ hereafter. We made use of the blue lines in Figure 1A as the limit sides of the features for a first estimation of the hyperfine constants. The extremal values for the hyperfine interaction of these limit sides would be:

$$(A_2)^{u1} = +13 \pm 2 \text{ MHz} \quad (A_2)^{u2} = -9 \pm 2 \text{ MHz} \tag{7}$$

for the upper line (indicated with the superscript "u"), and

$(A_2)^{l1} = +17 \pm 3$ MHz $(A_2)^{l2} = -7 \pm 2$ MHz (8)

for the lower one (superscript "*l*"). This would correspond to a rhombic hyperfine interaction, characterized by the parameters a, T and δ[28], of $^1H_2$ with the following two sets of compatible hyperfine parameters:

i) $T_2 = +8 \pm 2$ MHz	*or*	ii) $T_2 = +8 \pm 2$ MHz	
$\delta_2 = +3 \pm 3$ MHz		$\delta_2 = +3 \pm 3$ MHz	(9)
$a_2 = -9 \pm 5$ MHz		$a_2 = 0 \pm 4$ MHz	

where the principal values of the hyperfine tensor would be $(A_x)_2 = (a_2 - T_2 - \delta_2)$, $(A_y)_2 = (a_2 - T_2 + \delta_2)$, $(A_z)_2 = (a_2 + 2\,T_2)$.

Again the error values come from the HYSCORE signal width. These rather crude estimations were refined as it will be shown in the next section. Nevertheless, some first conclusions could be obtained such as hyperfine interactions of the Mn-cluster in the S_2 state with two ^1H nuclei were detected, one showing an axial ***A*** tensor and another a rhombic one. The anisotropic T constant is larger for the rhombic one, indicating that this nucleus is closer to the Mn-cluster than the one responsible for the axial interaction.

Refinement of the estimated hyperfine constants, comparison with previous ENDOR data and HYSCORE simulations.

The uncertainty between the two sets of hyperfine parameters can sometimes be resolved by analysing the intensities of the correlation ridge in the spectrum. To do that, we will pay attention to the *skyline projections* in Figure 2. Besides, comparison with previously reported ENDOR experiments[15-17,19] can also help to resolve the uncertainty and to determine the hyperfine constants more accurately, as some of the ENDOR features should correspond to the same interactions that cause our HYSCORE signals.

For a better understanding of the following analysis, we will first discuss the intensities and shapes of ENDOR and HYSCORE features. Intensities of ENDOR signals from orientationally disordered samples are mainly related with the symmetry of the hyperfine interaction. When the ***A*** tensor is axial, the most intense feature corresponds to the perpendicular orientation, and in many cases only the feature associated to $A_\perp$ is detected[17]. When the ***A*** tensor is rhombic, the feature corresponding to the intermediate principal value, (A_y), displays the most intense feature, and many times is again the only one detected. Intensities in HYSCORE experiments are more complex. They also depend on the tensor symmetry: positions near to $A_\perp$ or (A_y) are favoured in each case. However, the influence of the HYSCORE "modulation depth" must also be considered[21]. This is a function of the experimental τ value and the transition probabilities in the nuclear Hamiltonian. For the principal directions of the ^{1}H hyperfine tensors the modulation depth vanishes. Then, for axial hyperfine interactions, the combination of these two contributions causes the highest intensity of the HYSCORE features to be near the $A_\perp$ position, but not exactly in it. For a rhombic interaction, the position for the highest intensity is more difficult to be predicted, but will usually be near the intermediate A_y one.

We made use of these ideas to analyse *skyline projections* in Figure 2. For signal **1**, the highest intensity appears for a hyperfine parameter (estimated from the distance between the two maxima) $A \approx 3$ *MHz*. The two sets of hyperfine constants for this signal (Eq. 6) predict $A_\perp$ values of about 7 MHz or 2 MHz, respectively. The closest value corresponds to the ii) set, the one of the smallest $|a_I|$ value. In signal **2**, the highest intensity is displayed for a value of the hyperfine parameter $A \approx 5$ *MHz*.

These results can be compared with those obtained by other authors in ^{1}H ENDOR studies of the Mn-cluster S_2 state. Several authors have reported CW-ENDOR experiments on this system, where two main features that correspond to hyperfine parameters $A = 2.3$ *MHz* and $A = 4.0$ *MHz* were detected[15,16,19]. Besides, pulsed ENDOR spectra were reported[17] where those signals were seen, but additional signals also appeared: for instance, a well characterized shoulder shaped feature at about $A = 9$ *MHz*, a small contribution at about $A = 5.5$ *MHz*, and a weak contribution that spreads to values as

large as $A = 14\ MHz$. In those previous studies, the authors tried to assign these ENDOR signals to hyperfine interaction of ^{1}H nuclei near the Mn-cluster, but in all the cases axial hyperfine interactions were only considered. This is a logical restriction when no other evidences can be used, as it reduces the number of hyperfine constants to be determined from the experiments. However, it implies a severe limitation for describing the interactions that are actually taking place. In fact, in a system where the electronic spin is so spatially distributed as it is in the Mn-cluster, hyperfine interactions are in general rhombic even when the "point dipole approximation" is suitable (see Materials and Methods and [21]). Axial hyperfine interactions are only displayed by ^{1}H nuclei placed in the few positions where two of the principal values of the complete hyperfine tensor $(^{\mathbf{H}}\boldsymbol{A})_i$ coincide. This situation contrasts with the case of a ^{1}H nucleus interacting with an electronic spin well localized in an atom, where the hyperfine interaction in the "point dipole approximation" is always axial.

Our HYSCORE results have identified one ^{1}H nucleus with an axial interaction and another ^{1}H nucleus with a rhombic one, and have provided a first estimation of their hyperfine constants. We can now make use of the previously reported ENDOR results[15-17,19] to refine this estimation if we can assign the ENDOR features to our HYSCORE detected interactions.

As we have explained above, the position of highest intensity in the *skyline projection* of each HYSCORE signal should be close to their corresponding ENDOR features. We can then assign the ENDOR feature $A = 2.3\ MHz$ to $^1\mathbf{H_1}$ (whose highest intensity corresponds to $A \approx 3\ MHz$), and the ENDOR feature $A = 4.0\ MHz$ to $^1\mathbf{H_2}$ (as its highest intensity corresponds to $A \approx 5\ MHz$). Thus the value $(A_\perp)_\mathbf{1} = 2.3\ MHz$ can be selected. This allows us to select the set ii) of the hyperfine constants in (6) for $^1\mathbf{H_1}$, and to improve the accuracy of these values as now the error values mainly come from the ENDOR signals width:

$$T_\mathbf{1} = +2.9 \pm 0.5\ MHz \qquad (10)$$

$$a_\mathbf{1} = +0.6 \pm 0.6\ MHz$$

From the assignment of ENDOR $A = 4.0\ MHz$ feature to $^1H_2$, the intermediate principal value should be $(A_y)_2 = 4.0\ MHz$. This is only compatible with the set ii) of $^1H_2$ hyperfine constants in Eq. (9). This implies that the other two principal values of the hyperfine tensor of $^1H_2$ would then have larger absolute values than $(A_y)_2$, and that $(A_x)_2$ and $(A_z)_2$ should have opposite signs. Following an analysis similar to the one used by Aznar and Britt[17] for axial hyperfine interactions, we can draw the typical pulse ENDOR signal associated to this kind of rhombic interaction. It can be seen in Figures S6-S7 of Supporting Information. Besides the peak in the intermediate principal value position, the pulse ENDOR shape associated to such a rhombic hyperfine interaction shows two shoulders in the spectral intensity. The shoulder corresponding to the principal value closer to the intermediate one is very well characterized, whereas the other shoulder is weaker, similar to the one displayed by an axial hyperfine interaction in the $A_{||}$ position. This points to an alternative interpretation of the ENDOR results[17] by making use of the two hyperfine interactions detected in HYSCORE spectra, one axial and another rhombic. The shoulder at $A \approx 9\ MHz$ would not be assigned to a $A_{||}$ feature but to the A_x position of $^1H_2$, as its intensity seems quite more compatible with a shoulder of a rhombic interaction. The other shoulder of $^1H_2$ would be at $A \geq 13\ MHz$, and this would explain the signal at these positions without including an additional axial interaction, as other authors suggested[17]. The $A \approx 1\ MHz$ would be assigned, in our interpretation, to remote ^1H nuclei, whose contributions are also seen in CW-ENDOR spectra and in our HYSCORE experiments. A comparison between the aspects of ENDOR spectra obtained from both interpretations can be seen in Figure S7 of Supporting Information. We feel that our interpretation explains better the spectral shapes detected in the previously reported pulse ENDOR spectra[17]. Moreover, our interpretation is the only one that takes into account all the experimental evidence now available (CW-ENDOR, pulse ENDOR and HYSCORE).

From this analysis, and considering the ENDOR signals positions, the estimation of the hyperfine constants for $^1H_2$ can be refined:

$$T_2 = +6.7 \pm 1.0\ MHz$$

$$\delta_2 = +2.7 \pm 1.0\ MHz \qquad (11)$$

$$a_2 = +0.3 \pm 1.0\ MHz$$

In order to confirm our analysis, we used the refined hyperfine constants for simulating the HYSCORE spectra. A comparison between simulated and measured spectra at 338 mT and 370 mT is displayed in Figure 3. The good agreement of the simulations further supports the hyperfine constants obtained in our previous analysis.

There is also a "physical" support for the obtained hyperfine constants, as in both cases the isotropic contribution is small or negligible. This is the expected result for hyperfine interaction with ^{1}H nuclei that are at distances of 2.0 Å or larger and are not directly bound to atoms with noticeable spin density. Previous studies indicated that Mn-cluster in the S_2 state only show noticeable spin densities in the Mn atoms and in the oxygen atoms involved in the oxo-bridges between them[1,29]. Besides, the obtained hyperfine anisotropic constants point to distances to the paramagnetic center larger than 2.0 Å (see Discussion below).

DISCUSSION

Our analysis has allowed to identify hyperfine interaction of the Mn cluster with two ^{1}H nuclei and to estimate their corresponding hyperfine constants within a fair accuracy. This information can be useful for answering several key questions about the function of the OEC[4], particularly about the structure of the Mn-cluster and the presence of water molecules in the S_2 state. The interpretation of these results requires a "microscopic" model on the atomic and spin spatial distributions in the Mn-cluster center. In the last years, data from X-ray diffraction[2,30,31] and EXAFS[10,32,33], and results from several calculations[1,3,29] have been handled to obtain the structure of the Mn-cluster in the different S_i states, particularly in the S_2 one. That evidence seems to be difficult to reconcile, and nowadays there is not a unique structural model but several proposals that can be considered more or less compatible with the literature data. Those models differ in several details, such as the positions of Ca, Cl and oxo-bridge atoms, although the Mn-Mn distances are quite preserved among them. Some of them also place several

water molecules in the structure for the S_2. When the water molecules are near to the Mn atoms, their ^{1}H nuclei are indeed candidates to be responsible of the hyperfine interactions detected by HYSCORE and ENDOR.

The hyperfine interactions can be calculated when the knowledge about the positions of the Mn atoms and ^{1}H nuclei is combined with a model for the electronic spin distribution. The latter has been established in the last years, mainly from data on the ^{55}Mn hyperfine interaction detected in the Mn-cluster S_2 state by using CW-EPR and ENDOR techniques[4,7,11,13]. The "total" spin S_T comes from the combination of the individual spins of the four Mn atoms that are coupled by magnetic exchange interactions. The hyperfine interaction of the total spin with the four ^{55}Mn nuclei causes the splitting of the MLS in CW-EPR spectra and the corresponding features in ^{55}Mn ENDOR spectra. The "effective" hyperfine interaction is related with the interaction of each nucleus with its own individual electronic spin through four "projection matrices" (that for some descriptions can be approximated to "projection constants") accomplishing:

$$^{hf}H(^{55}\mathrm{Mn}) = \boldsymbol{S_T}\ \Sigma_i\ (^{Mn}\boldsymbol{A})_i\ (^{Mn}\boldsymbol{I})_i \qquad \text{(i from 1 to 4)} \qquad (12)$$

$$(^{Mn}\boldsymbol{A})_i = \rho_i\ (^{Mn}\boldsymbol{a})_i$$

where $^{hf}H(^{55}\mathrm{Mn})$ is the part of the spin Hamiltonian giving account of the hyperfine interaction with the four ^{55}Mn nuclei, $\boldsymbol{S_T}$ is the total spin, $(^{Mn}\boldsymbol{A})_i$ are the "effective" hyperfine tensors (i. e., the tensors describing the interaction with the total spin responsible for the actual spectral hyperfine splitting), $(^{Mn}\boldsymbol{I})_i$ are the nuclear spins of each ^{55}Mn nucleus ($^{Mn}\boldsymbol{I} = 5/2$), $(^{Mn}\boldsymbol{a})_i$ is the hyperfine tensor that describes the interaction of each Mn individual electronic spin with its own nucleus, and ρ_i are the "projection matrices" (or constants) (see Materials and Methods).

A suitable estimation of ρ_i requires the knowledge of the total spin S_T, the "coupling scheme" of the individual spins, and the individual $(^{Mn}\boldsymbol{a})_i$ tensors. The latter has been estimated from model compounds[7,13]. Concerning the total spin, it is well established that in the S_2 state, $S_T = ½$. Nevertheless,

there is many ways for a cluster of four Mn atoms to reach a ground state S_T = ½, depending on the individual spins and the values of the magnetic exchange constants that couples each pair of Mn atoms. The experimental hyperfine splittings and other "physical" constraints of the systems were used to estimate the actual "coupling scheme" and the projection constants. The conclusions of those studies[1,3,7,13] can be summarized as follows:

a) In the S_2 state, most authors consider that three Mn atoms have oxidation number IV and one has III.

b) The most accepted "coupling schemes" are "trimer-monomer" (also known as "Dangler model"[4,12]), where three Mn atoms are strongly coupled, and one "dangling" Mn interacts with the trimer through just one "magnetic path" (characterized by one exchange constant). One of the most used "Dangler model" schemes was proposed by Kulik et al.[3,7], and shows a chain of strong antiferromagnetic coupling constants with an additional, weaker coupling constant within the trimer.

c) The position of the Mn(III) in the cluster has not been yet resolved; models where the Mn(III) is placed in the "dangling" Mn position, or in different positions into the trimer, have been proposed[3,7,13,14].

d) The model from Kulik et al.[7] suggests that the sign of the spin population in each Mn atom (i.e., the sign of the projection constants) alternates within the "antiferromagnetic chain", as other studies have proposed[13].

e) Wherever the Mn(III) atom is placed within the cluster, the absolute value of its projection constant seems to be larger (between 30% to 90%) than those of the Mn(IV) ones, which have similar absolute values between them.

f) The projection constants ρ_i obtained from ^{55}Mn hyperfine interaction studies can be directly used to calculate the ^{1}H hyperfine interactions. If ^{1}H nucleus is placed at about 2.4 Å or farther, the "point dipole approximation" applies, and the hyperfine tensor can be calculated and compared with the experimental one, by means of Eqs. (1) to (5) in Materials and Methods[16].

In order to illustrate the use of the ^{1}H hyperfine parameters as a structural tool, we will undertake some calculations in a specific model. As the structure of the Mn-cluster we will make use of the "model III" by Yano et al.[3,32], mainly based on EXAFS data. The model includes several water molecules, and we will pay attention to those previously considered as functionally relevant[29]. Besides, a "Dangler model" with sign-alternating projection constants will be considered. We will also assume that Mn(III) is placed in the "dangling position", although calculations are not very sensitive to such a particular choice, as we will show later. Figure 4 displays the main details of the selected model.

As we have previously indicated, the ^{1}H hyperfine tensors can be calculated by adding the contribution of each Mn spin population. It is worth of noting that when the distance between the nuclear and the electronic spins is longer than 7 Å, there is not a significant contribution to the hyperfine tensor. As the electronic spin is distributed in an extended region (the longest distance between two Mn atoms is around 5.3 Å), for many ^{1}H nucleus positions the total hyperfine interaction can be calculated from the contribution of just two, or three, of the Mn atoms. For this reason, it is interesting to discuss a simplified model, where only the interaction with two Mn atoms is considered[16]. In this case, the relevant geometry details are outlined in Figure 5.

We can explore the positions for the ^{1}H nuclei that would display hyperfine constants compatible with our results for $(^1H)_1$ and $(^1H)_2$. As it can be seen in Figure 5, the model shows a rotational symmetry around the Mn-Mn axis, thus each position compatible in the plane of Figure 5 implies a set of positions forming a circumference around this axis.

$(^1H)_1$ displays an axial hyperfine interaction (within the accuracy of our estimation). As we discussed above, it imposes an important restriction on the compatible positions for the ^{1}H nucleus. When calculating in the "point dipole approximation", each one of the two contributions to the total hyperfine tensor $(^H\boldsymbol{a})_j$ is axial, but in general it is not that way for the $(^H\boldsymbol{A})$ tensor, as the two $(^H\boldsymbol{a})_j$ tensors do not have common principal directions. In Figure 5, one principal direction for the two $(^H\boldsymbol{a})_j$ tensors is perpendicular to the drawn plane, and for each $(^H\boldsymbol{a})_j$ the two other principal directions are parallel and perpendicular to the d_j directions within the plane. Consequently, it is easy to see that points lying on the

Mn1-Mn2 direction will display axial $(^{H}\boldsymbol{A})$ tensor as in these positions the principal directions of the $(^{H}\boldsymbol{a})_j$ coincide. Other positions close to these will display nearly axial $(^{H}\boldsymbol{A})$ tensors, and will be compatible with the experimentally determined hyperfine constants. Then, compatible positions around the Mn-Mn direction will seem a spherical cap. Other few compatible positions could appear when an incidental coincidence of two principal values of $(^{H}\boldsymbol{A})$ occurs.

As an example, Figure 6 shows a calculation of the positions compatible with the obtained hyperfine constant of $(^1\mathrm{H})_1$ in the "two Mn" model. Two characteristic caps are observed, which are placed at a distance around 3 Å of the closest Mn atom. It is worth of noting that the compatible ^{1}H positions are almost not influenced by the actual values of the projection constants of the two Mn atoms. On the other hand, the relative signs of both constants are relevant, as the resulting compatible positions for a model with the same projection constants signs are very different from one with alternating projection constants signs. Figure 6 shows that a 50% change in the absolute value of ρ_1 causes a change in the ^{1}H-Mn distance of only 0.3 Å.

When more than two Mn atoms are considered, the angular extent of these spherical caps of compatible positions will be reduced, as the additional contributions will in general break down the axial symmetry of the $(^{H}\boldsymbol{A})$ tensor. In the four-Mn model of Figure 4, the compatible positions for $(^1\mathrm{H})_1$ would be mainly distributed as small caps near to each Mn atom, out of the Mn-cluster "pocket" formed by the four Mn and the Ca atoms. Only the one near Mn1 (the "dangling" position) could be associated to a water molecule into this pocket.

Similar calculations in the "two Mn" model can be done to determine the positions compatible with $(^1\mathrm{H})_2$ (Figure 7). These positions form rings around the Mn-Mn direction. The radius of the rings is about 2.1-2.4 Å, their center is close to the Mn atom position, and the distance to the closest Mn atom is about 2.4 Å. This is in the limit of the validity of "point dipole approximation", indicating that our calculations could be considered suitable. Again the positions are not very sensible to the actual value of ρ_i within a model of alternating signs. The position and shape of these rings are changed when four Mn atoms are included in the calculation (results not shown), in such a way that still a ring could be

identified around Mn1, but compatible positions in other places of the Mn cluster do not display any specific shape.

The above described model can also be used for calculating the hyperfine constants of ^{1}H nuclei at specific positions. We will show these calculations for W1, W2 and W3 water molecules in Figure 4[3,29], in order to compare them with the experimental results. To assign the detected hyperfine interactions, it has to be taken into account that a water molecule has two ^{1}H nuclei that can in principle interact with the electronic spin. We can calculate the hyperfine interaction for both. It has been postulated that $(^1H)_1$ and $(^1H)_2$ are bound to different molecules[19]. Then, if one of the ^{1}H nuclei in a water molecule is compatible with one of the experimental values, we also have to understand why the other one is not detected. There are several situations where the second ^{1}H would not be detected:

a) If the second ^{1}H nucleus is farther away from Mn atoms than the other, its hyperfine interaction can be weak, and it would be hidden into the "remote ^{1}H" signal both in ENDOR and HYSCORE experiments.

b) Even if the second ^{1}H is not far from the Mn atoms, the hyperfine interaction could be largely rhombic, in such a way that the main spectral feature (corresponding to the intermediate principal value of the $(^H\boldsymbol{A})$ tensor) would be again hidden into the "remote ^{1}H" signal.

c) The second ^{1}H could be placed in another compatible position, and would display the same hyperfine constants (within the experimental accuracy) of one of the detected ^{1}H nucleus.

d) The second ^{1}H could have different hyperfine constants from the detected ones, but its signal could be superimpose. For example, an interaction with the main ENDOR feature around 4 MHz would be surely not resolved in the ENDOR measurements and would also be hidden by the more intense $(^1H)_2$ HYSCORE feature.

e) The "water molecule" in the model could actually be an OH^- ion, with only one H atom.

With these ideas in mind, we have calculated the hyperfine constants for the positions of the two ^{1}H nuclei, *a* and *b*, of the three water molecules in Figure 4 [3] for a set of projection constants (Table 1). It has to be taken into account that the projection constants values can be different, specially if the Mn(III)

atom is in another position, although we have seen that changes in the absolute values of the projection constants preserving the alternating signs model have small effect on the calculated hyperfine constants, and also that the positions of the ^{1}H nuclei in the structure are tentative as they are not determined from the experiments.

We will discuss the results for each water molecule separately:

-W1: The molecule is placed near Mn1 and Mn2 atoms. ^{1}H(W1a) nucleus is compatible with the experimental hyperfine constants of $(^1H)_{\mathbf{2}}$. This nucleus would be placed in the compatible ring around Mn1 (see Figure 7). On the other hand, ^{1}H(W1b) nucleus is nearly to the same distance of Mn1 and Mn2. It is placed in one of the incidental positions where the ($^H\boldsymbol{A}$) tensor becomes axial (see above). As its hyperfine principal values are similar to two of the ones calculated for ^{1}H(W1a), its ENDOR and HYSCORE features could be hidden in the spectra. Besides, it has to be also taken into account that, in the region in between Mn1 and Mn2 atoms, a very small change in the ^{1}H position would cause a large shift of the hyperfine constants, specially δ, and in such a case the resulting, very rhombic interaction would be not detected.

W2: The closest Mn atom is Mn1. The distance Mn1-O(W2) is about 3.9 Å. However, as one ^{1}H(W2a) is directed to Mn1, it is placed within the spherical cap of $(^1H)_{\mathbf{1}}$ compatible positions (Figure 6). The other ^{1}H(W2b) is farther apart from the Mn-cluster and can be considered a remote ^{1}H nucleus.

W3: This molecule is close to Mn4 (distance Mn4-O(W3) = 2.2 Å). The ^{1}H(W3b) nucleus is nearly within the spherical cap of $(^1H)_{\mathbf{1}}$ compatible positions around Mn4. The other ^{1}H(W3a) nucleus displays a very rhombic hyperfine tensor, that would be not resolved in the ENDOR and HYPERFINE measured spectra, as we have indicated above (point b).

We have seen that the three water molecules are quite compatible with the ENDOR and HYSCORE experimental evidence. Our simulation point out the possibility that some spectral signals could come from several hyperfine interactions, which could perhaps explain the results of previously reported ^{2}H-ESEEM studies[18]. Nevertheless, any structural model of the S_2 state Mn-cluster including water molecules should be compatible with these obtained hyperfine couplings.

CONCLUSIONS

Summarizing, we have obtained quite accurate ^{1}H hyperfine couplings for the S_2 state of the Mn-cluster of PSII from new HYSCORE experiments and the comparison with previously reported ENDOR measurements. These couplings have been explained on the basis of the current structural and spin models for the Mn-cluster. This provides additional evidence to improve our knowledge of the OEC functioning.

ACKNOWLEDGEMENTS

This work was supported by Spanish Ministry of Science and Innovation (projects MAT2008-03461 and AGL2008-00377) and Gobierno de Aragón (DGA-GC E33 and DGA-GE B18).

Supporting information available: Selected magnetic field positions within the MLS for HYSCORE measurements are given in figure S1. Comparison between HYSCORE spectra from dark (S_1) and illuminated (S_2) samples are displayed in Figures S2 to S5. The shape of absorption mode ENDOR spectra from axial and rhombic hyperfine couplings are shown in Figure S6, and a comparison between calculated ENDOR spectra from three axial hyperfine couplings and one axial and one rhombic hyperfine couplings is displayed in Figure S7. This material is available free of charge via the Internet at http://pubs.acs.org.

REFERENCES

(1) Sproviero, E. M.; McEvoy, J. P.; Gascón, J. A.; Brudvig, G. W.; Batista, V. S. *Photosynth. Res*. **2002**, *97*, 91-114.

(2) Barber, J.; Murray, J. W. *Phil. Trans. R. Soc. Lond. B* **2008**, *363*, 1129-1138.

(3) Zein, S.; Kulik, L. V.; Yano, J.; Kern, J.; Pushkar, Y.; Zouni, A.; Yachandra, V. K.; Lubitz, W.; Neese, F.; Messinger, J. *Phil. Trans. R. Soc. Lond. B* **2008**, *363*, 1167-1177.

(4) Peloquin, J. M.; Britt, R. D. *Biochim. Biophys. Acta* **2001**, *1503*, 96-111.

(5) Goussias, C.; Boussac, A.; Rutherford, A. W. *Phil. Trans. R. Soc. Lond. B* **2002**, *357*, 1369-1381.

(6) McEvoy, J.; Brudvig, G. W. *Chemical Reviews* **2006**, *106*, 4455-4483.

(7) Kulik, L. V.; Epel, B.; Lubitz, W.; Messinger, J. *J. Am. Chem. So*c. **2007**, *129*, 13421-13435.

(8) Hendry, G.; Wydrzynski, T. *Biochemistry* **2002**, *41*, 13328-13334.

(9) Britt, R. D.; Peloquin, J. M.; Campbell, K. A. *Annu. Rev. Biophy. Biomol. Struct*. **2000**, *29*, 463-495.

(10) Yano, J.; Yachandra, V. K. *Photosynth. Res*. **2007**, *92*, 289-303.

(11) Zheng, M., Dismukes, G. C. *Inorg. Chem.* **1996**, *35*, 3307-3319.

(12) Peloquin, J. M.; Campbell, K. A.; Randall, D. W.; Evanchik, M. A.; Pecoraro, V. L.; Armstrong, W. H.; Britt, R. D. *J. Am. Chem. So*c. **2000**, *122*, 10926-10942.

(13) Charlot, M.-F.; Boussac, A.; Blondin, G. *Biochim. Biophys. Acta* **2005**, *1708*, 120-132.

(14) Pantazis, D. A.; Orio, M.; Petrenko, T.; Zein, S.; Lubitz, W.; Messinger, J.; Neese, F. *Phys. Chem. Chem. Phys*. **2009**, *11*, 6788-6798.

(15) Kawamori, A.; Inui, T.; Ono, T.; Inoue, Y. *FEBS Lett*. **1989**, *254*, 219-224.

(16) Fiege, R.; Zweygart, W.; Bittl, R.; Adir, N.; Renge, G.; Lubitz, W. *Photosynth. Res*. **1996**, *48*, 227-237.

(17) Aznar, C. P., Britt, R. D. *Phil. Trans. R. Soc. Lond. B* **2002**, *357*, 1359-1365.

(18) Britt, R. D.; Campbell, K. A.; Peloquin, J. M.; Gilchrist, M. L.; Aznar, C. P.; Dicus, M. M.; Roblee, J.; Messinger, J. *Biochim. Biophys. Acta* **2004**, *1655*, 158-171.

(19) Yamada, H.; Mino, H.; Itoh, S. *Biochim. Biophys. Acta* **2007**, *1767*, 197-203.

(20) Martínez, J. I., Alonso, P. J., Gómez-Moreno, C., Medina, M. *Biochemistry* **1997**, *36*, 15526-15537.

(21) Schweiger, A.; Jeschke, G. *Principles of Pulse Electron Paramagnetic Resonance*. Oxford University Press: Oxford, 2001.

(22) García-Rubio, I.; Martínez, J. I.; Picorel, R.; Yruela, I.; Alonso, P. J. *J. Am. Chem. Soc.* **2003**, *125*, 15846-15854.

(23) Berthold, D. A.; Babcock, G. T.; Yocum, C. F. *FEBS Lett*. **1987**, *134*, 231-234.

(24) Miller, A-F; Brudvig, G. W. *Biochim. Biophys. Acta* **1991**, *1056*, 1-18.

(25) Haddy, A. *Photosynth. Res*. **2007**, *92*, 357-368.

(26) Spaeth, J. M.; Niklas, J. R.; Bartram, R. H. *Structural Analysis of Point Defects in Solids. An Introduction to Multiple Resonance Spectroscopy*; Springer: Berlin, 1992; Ch. 6.

(27) Degliannakis, Y.; Ivancich, A.; Rutherford, A. W. *Spectrochim Acta. Part A* **2002**, *58*, 1191-1200.

(28) Dikanov, S. A.; Bowman, M. K. *J. Mag. Reson., Ser. A* **1995**, *116,* 125-128.

(29) Sproviero, E. M.; Shinopoulos, K.; Gascón, J. A.; McEvoy, J. P.; Brudvig, G. W.; Batista, V. S. *Phil. Trans. R. Soc. Lond. B* **2008**, *363*, 1149-1156.

(30) Ferreira, K. N.; Iverson, T.; Maghlaoui, K.; Barber, J.; Iwata, S. *Science* **2004**, *303*, 1831-1838.

(31) Loll, B.; Kern, J.; Saenger, W.; Zouni, A.; Biesiadka, J. *Nature* **2005**, *438*, 1040-1044.

(32) Yano, J.; Kern, J.; Sauer, K.; Latiner, M. J.; Pushkar, Y.; Biesiadka, J.; Loll, B.; Saenger, W.; Messinger, J.; Zouni, A.; Yachandra, V. K. *Science* **2006**, *314*, 821-825.

(33) Yano, J.; Kern, J.; Pushkar, Y.; Sauer, K.; Glatzel, P.; Bargmann, U.; Messinger, J.; Zouni, A.; Yachandra, V. K. *Phil. Trans. R. Soc. Lond. B* **2008**, *363*, 1139-1147.

Table 1. Calculated hyperfine constants T and δ for ^{1}H nuclei in Figure 4. The set of projection constants has been selected on the basis of previous works[7,13], assuming the Mn(III) is the "dangling" Mn (Mn1).

	$\rho_1 = 1.3, \rho_2 = -0.9, \rho_3 = 1.0, \rho_4 = -0.9$		
	T (MHz)	δ (MHz)	A_x, A_y, A_z (MHz)
W1a	7.1	2.5	-9.6, -4.6, 14.2
W1b	4.8	0.1	-4.9, -4.7, 9.6
W2a	2.5	0.5	-3.0, -2.0, 5.0
W2b	0.9	0.4	-1.4, -0.5, 1.9
W3a	3.3	2.0	-6.6, 1.3, 5.3
W3b	3.0	0.8	-5.9, 2.1, 3.8

FIGURE CAPTIONS

Figure 1. Detail of the "^{1}H region" of the Mn-cluster S_2 state HYSCORE spectra at two different magnetic field positions. A) 338 mT, B) 370 mT. Correlations assigned to $^1H_1$ and $^1H_2$ (see text) are identified by numbers. In Figure 1A, dashed blue lines indicate the estimated limits for signal **2** (see text). See Material and Methods for experimental conditions.

Figure 2. "Skyline projections" of the two signals **1** and **2** detected in the HYSCORE spectrum of Mn-cluster in the S_2 state at 338 mT. The projections were obtained as follows: all the spectral contributions, except signal **1** or **2**, were erased from the 2D frequency spectrum of Figure 1A. Then, 1D profiles of the signal projected on the ω_1 and ω_2 axes were obtained.

Figure 3. Comparison between measured (black line) and simulated (red line) HYSCORE spectra for two magnetic field positions: A) 338 mT, B) 370 mT. Simulation parameters were: τ = 200 ns; hyperfine constants: $(a)_1 = 0.0$ MHz, $(T)_1 = 2.9$ MHz, $(\delta)_1 = 0.0$ MHz; $(a)_2 = 0.0$ MHz, $(T)_1 = 6.8$ MHz, $(\delta)_1 = 2.8$ MHz.

Figure 4. Image of the atoms positions in the "model III" of Mn-cluster[3]. Atom colour code: purple: manganese; red: oxygen; brown, calcium; blue: hydrogen. Three water molecules, previously considered as relevant for OEC function, have been included. Distances Mn1-Mn2, Mn2-Mn3 and Mn3-Mn4 are about 2.7 Å. Distances Mn-Ca are all between 3.5 Å and 4.0 Å.

Figure 5. Simplified model of two Mn atoms and one ^{1}H nucleus for hyperfine tensor calculations. For a given Mn-Mn distance (2.7 Å), ^{1}H distances to Mn1 and Mn2, d_1 and d_2, the orientations of these segments, and projection constants ρ_1 and ρ_2, are the input data. Note that the results are symmetric under rotation around the Mn1-Mn2 direction (see text).

Figure 6. Positions of a ^{1}H nucleus compatible with $(^1H)_1$ ($T_1 = 2.9 \pm 0.5$ MHz, $\delta_1 = 0.0 \pm 0.5$ MHz) in the "two Mn" model of Figure 5, for two couples of projection constants values.

Figure 7. Positions of a ^{1}H nucleus compatible with $(^{1}H)_2$ ($T_2 = 6.7 \pm 1.0$ *MHz*, $\delta_1 = 2.7 \pm 1.0$ *MHz*) in the "two Mn" model of Figure 5, for two couples of projection constants values.

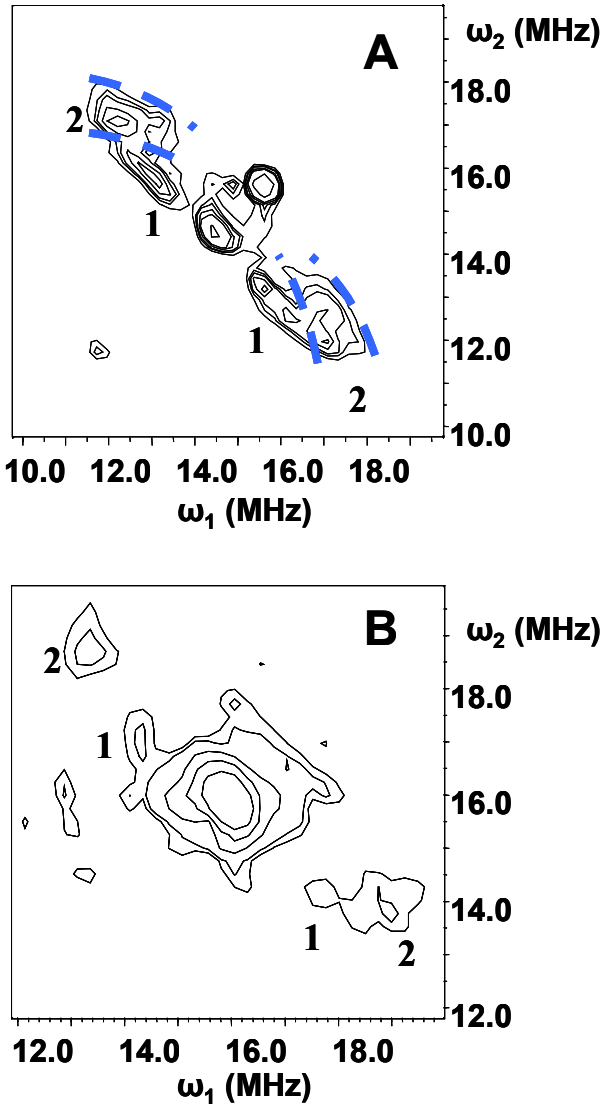

FIGURE 1

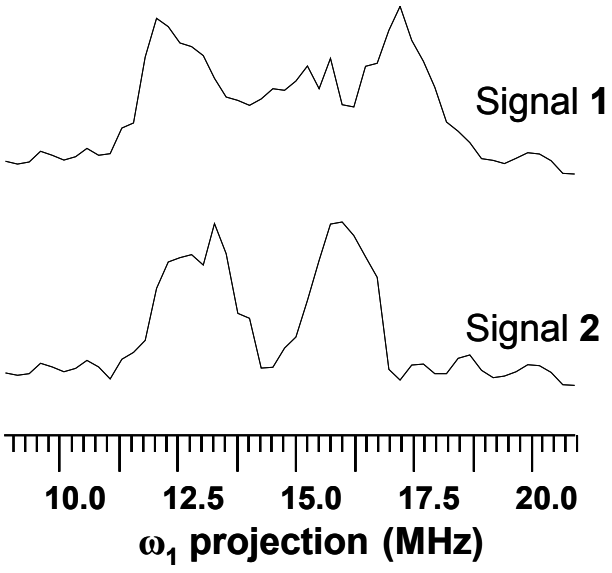
Signal 1
Signal 2
10.0
12.5
15.0
17.5
20.0
ω1 projection (MHz)

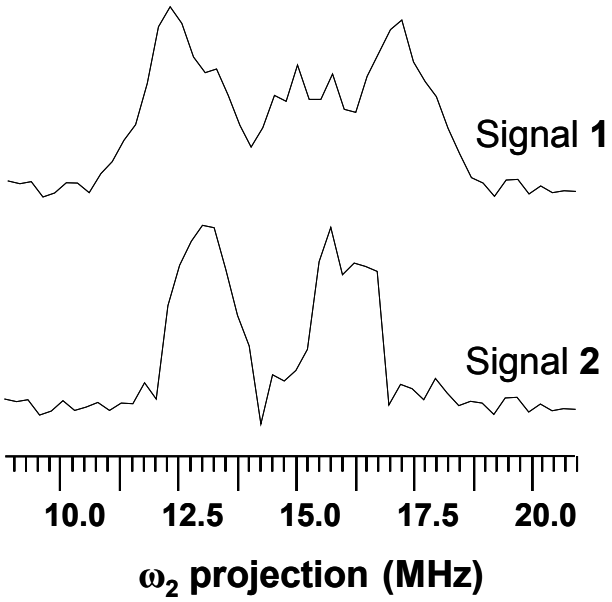
Signal 1
Signal 2
10.0
12.5
15.0
17.5
20.0
ω2 projection (MHz)

FIGURE 2

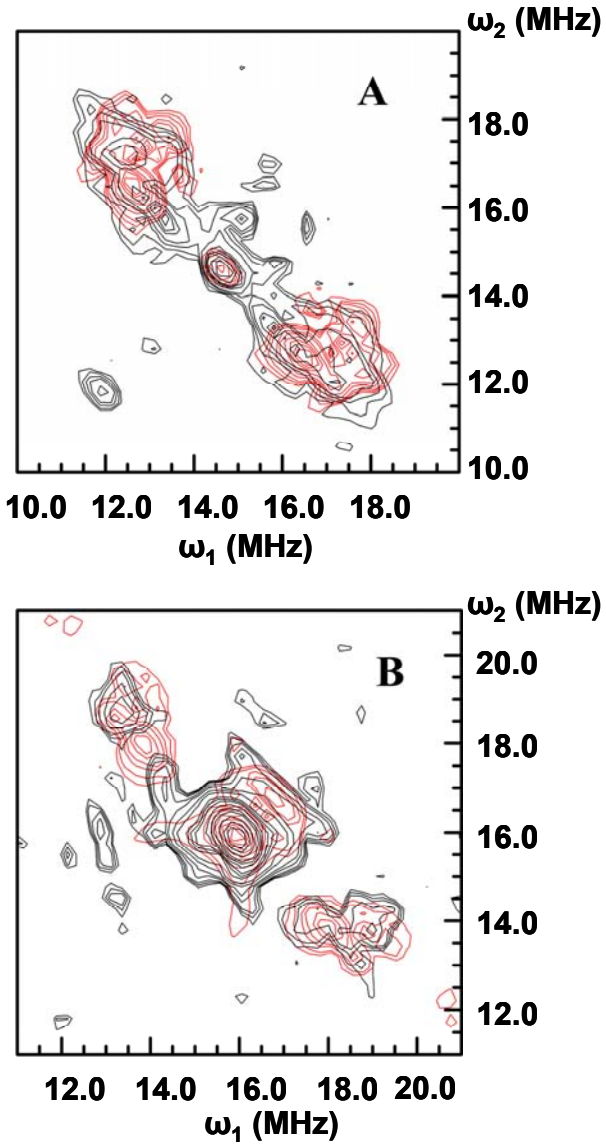
A
ω2 (MHz)
18.0
16.0
14.0
12.0
10.0
10.0 12.0 14.0 16.0 18.0
ω1 (MHz)
B
ω2 (MHz)
20.0
18.0
16.0
14.0
12.0
12.0 14.0 16.0 18.0 20.0
ω1 (MHz)

FIGURE 3

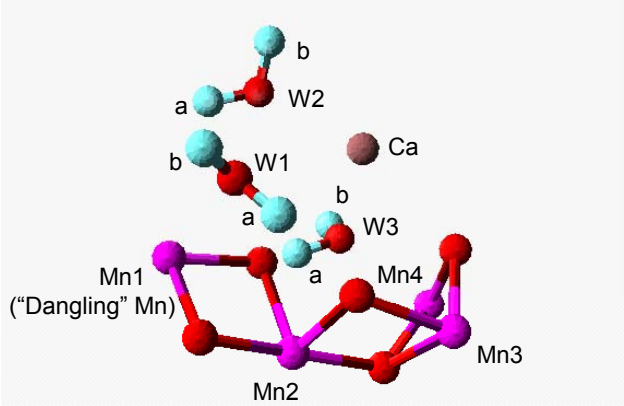

FIGURE 4

.

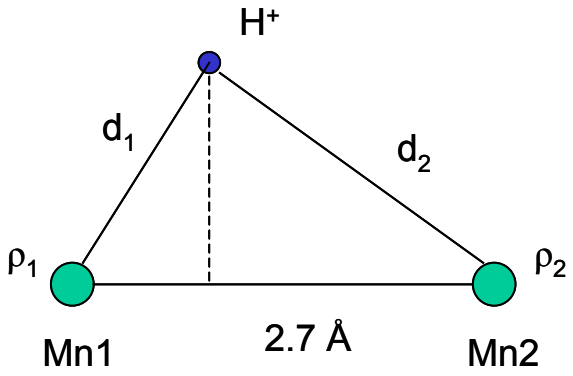

FIGURE 5

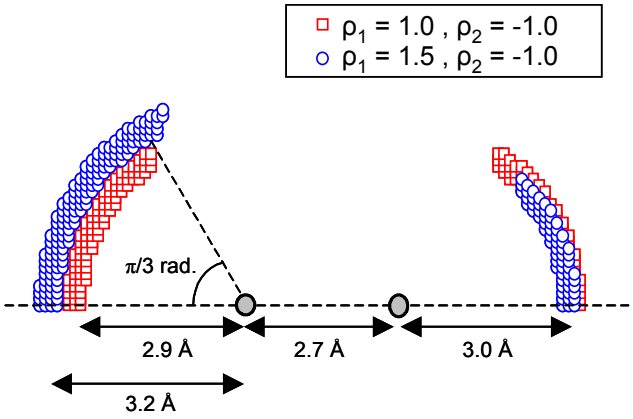

FIGURE 6

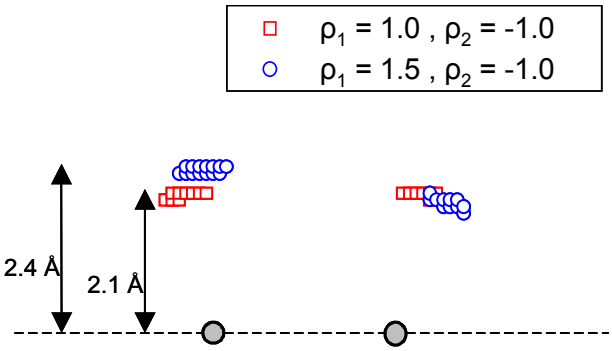

FIGURE 7

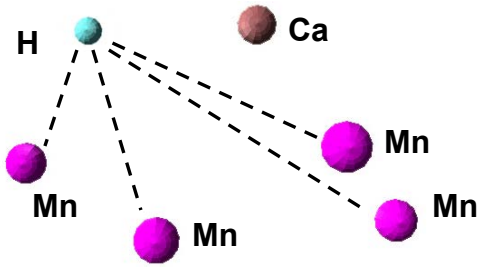

TOC graphic